# Generating a thermal squeezed phonon laser via nonlinear optomechanical interaction

Guoyao Li (李国耀)[1,2], Xintao Song (宋新涛)[1,2], Tengfang Kuang (邝腾芳)[1,2], Guangzong Xiao (肖光宗)[1,2,*] and Hui Luo (罗晖)[1,2,†]

[1]College of Advanced Interdisciplinary Studies, National University of Defense Technology, Changsha, Hunan 410073, China

[2]Nanhu Laser Laboratory, National University of Defense Technology, Changsha, Hunan 410073, China

2026 年 8 月 19 日

**Abstract**

As a valuable resource of coherent phonons with high coherence, narrow linewidth, and strong intensity, phonon laser holds significant potential for advancing information storage, topology simulation, phonon time crystal, and high-precision acoustic sensing. Limited by the thermal fluctuations, generating a squeezed phonon laser remains challenging. We theoretically consider a cavity optomechanical system in an unresolved sideband regime. Remarkably, without any feedback control or detuning modulation, the thermal squeezed phonon laser could be generated through the nonlinear optomechanical interaction. Although in a large damping rate, the maximum thermal squeezing is available as the mechanical oscillator is driven toward dynamical instability. Our work unlocks an innovation platform to explore the coherent manipulation on a macroscopic scale, promoting the development of phonon-laser sensing technologies.

**Keywords: Phonon Laser; Squeezing; Optomechanics;**

**PACS:** 42.50.Pq, 03.67.Mn

## 1. Introduction

Optomechanics, investigating the interaction between photons and phonons, has emerged as a highly productive field with significant scientific breakthroughs, including precision sensing [1–4], exploring the boundary between the classical and quantum [5–7], engineering macroscopic quantum state [8–10], implementing the advanced quantum information processing [11–13]. Recently, optomechanics serves as a versatile medium for realizing phonon laser by feedback control [14,15],nonreciprocity [16,17], stimulated optical supermode [18], and dissipative coupling [19–22]. Under the injection-locking technique, the

*Corresponding author. xiaoguangzong@nudt.edu.cn

†Corresponding author. luohui.luo@163.com

brightest multicolor phonon laser to date has been realized, with the fundamental mode amplified by three orders of magnitude and stable operation maintained for several hours [20]. Moreover, the frequency comb of phonon laser is also demonstrated within the four-wave mixing and Floquet engineering [21,22]. These advancements indicate that phonon laser holds significant scientific value and broad application potential across multiple disciplinary fields, including quantum optics, micro-nano photonics, and precision metrology [23].

In order to achieve a higher sensitivity in weak signal detection, sensor is prepared to a squeezed state, where the uncertainty of one conjugate quadrature is lower or higher than the other [24–26]. The experimental demonstration of squeezing in both thermal and ground states has been achieved via parametric squeezing [27,28], post-selection [29,30], pulse modulation [31–33], reservoir engineering [34–36], superconducting qubits [24,37], etc. However, squeezing a phonon laser in an open system is still a challenge for the thermal fluctuations. Because the frequency of phonons is much lower than that of photons, phonons prefer to couple with the thermal environment, rendering them more vulnerable to the thermal fluctuations [38]. The coherent phonons will be thermalized and the correlation can no longer be sustained. Even the phonon laser is squeezed via some operations, it will rapidly annihilate under the thermal fluctuations, whether in quantum or classical configurations. Limited by the decoherence, the generation of squeezed phonon lasers at larger scales remains a significant challenge [39].

In order to achieve a squeezed phonon laser in a general way, we resort to the optomechanics. It can coherently drive the mechanical oscillator from a thermal motion to a coherent behavior [19–22]. Based on this, we propose a practical scheme to realize a squeezed phonon laser in an unresolved sideband regime, where the cavity decay rate is larger than the mechanical frequency [40]. We improve the nonlinear optomechanical interaction by the driving power, dispersive coupling, and cavity quality [38]. From the perspective of the second-order coherence and the distribution of the effective phonon number, the enhanced nonlinear optomechanical interaction leads to a dynamical phase transition [19,41,42]. With the driving power up to the threshold value, the phonon laser occurs. Furthermore, we found that the generated phonon laser is also thermally squeezed by the enhanced nonlinear optomechanical interaction. The maximum thermal squeezing of the phonon laser occurs when the dynamics of the mechanical oscillator approaches instability. [43–45]. This theoretical proposal features inherent flexibility and conciseness, requiring no additional feedback control or detuning modulation. It creates unique conditions for studying the coherent manipulation in macroscopic regimes.

## 2. Dynamics of the system

As shown in Fig. 1 (a), we theoretically consider a typical optomechanical system comprising an optical cavity and a mechanical oscillator. Cavity field and mechanical oscillator inevitably couple to the thermal environment with the dissipation rates $\kappa$ and $\gamma_m$, respectively. Without the driving laser, the motion of the mechanical oscillator is dominated by the thermal environment, showing the stochastic Brownian motion. When the driving laser is injected into an optical cavity, the cavity field is coherently

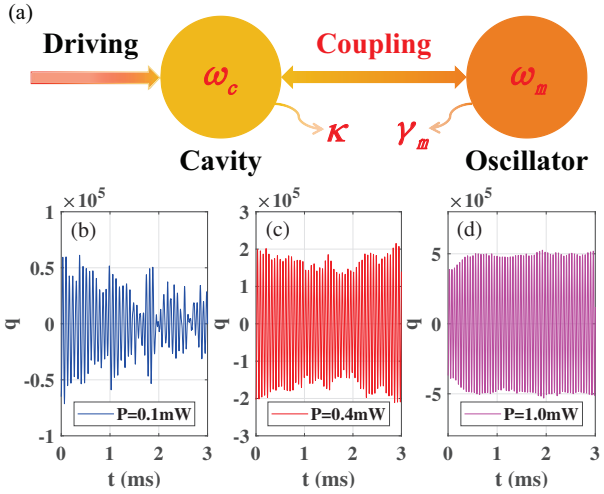



Fig. 1: (a) Schematic diagram for a typical cavity optomechanical system. The dimensionless displacement $q$ as a function of the evolution time $t$ with power $P = 0.1$ mW (b), $P = 0.4$ mW (c), and $P = 1.0$ mW (d). Experimental parameters are given as: mechanical oscillator frequency $\omega_m = 2\pi \times 14.4 \times 1000$ rad $\cdot$ Hz, oscillator mass $m = 1.0 \times 10^{-11}$ $kg$, mechanical damping rate $\gamma_m = 2\pi \times 1000$ rad $\cdot$ Hz, laser wavelength $\lambda = 1064$ nm, optomechanical coupling $g = 1.2 \times 10^{12}$ Hz/m, cavity quality factor $Q_c = 1.0 \times 10^9$, cavity-driving detuning $\Delta = 0$, environment temperature $T = 300$ K. With these experimental parameters, the system operates in both unresolved sideband regime ($\kappa \approx 20\omega_m \gg \omega_m$) and weak coupling regime ($G \approx 10^{-5}\omega_m \ll \kappa$).

excited. Under the optical force exerted by the cavity field, the mechanical oscillator can be driven from the thermal motions to the coherent oscillation.

In our assumption, both the cavity field and the motion of mechanical oscillator are Gaussian. The cavity field (motion of the mechanical oscillator) can be depicted by the bosonic creation operator $\hat{a}^\dagger(\hat{b}^\dagger)$ and annihilation operator $\hat{a}(\hat{b})$, satisfying the commutation relation $[\hat{a}^\dagger, \hat{a}] = 1$ ($[\hat{b}^\dagger, \hat{b}] = 1$). In this work, we focus on the dynamics of the motional mechanical oscillator. For convenience, the bosonic operators $\hat{b}$ and $\hat{b}^\dagger$ are decomposed to the dimensionless displacement operator $\hat{q}$ and the momentum operator $\hat{p}$ via canonical quantization. In such a situation, the dimensionless displacement operator $\hat{q}$ and the momentum operator $\hat{p}$ yielding the commutation relation $[\hat{q}, \hat{p}] = i$. Then, we can now characterize the model by the following Hamiltonian [38]

$$\begin{aligned}\hat{H} =& \hbar\omega_c \hat{a}^\dagger \hat{a} + \frac{1}{2}\hbar\omega_m \left(\hat{p}^2 + \hat{q}^2\right) - \hbar G \hat{a}^\dagger \hat{a}\hat{q} \\ &+ i\hbar E \left(\hat{a}^\dagger e^{-i\omega_l t} - \hat{a} e^{i\omega_l t}\right),\end{aligned} \tag{1}$$

where $G = gq_0$ represents the optomechanical coupling strength and $E = \sqrt{P\kappa/\hbar\omega_l}$ denotes the amplitude of the driving laser. The coupling coefficient $g$ quantifies the dispersive coupling rate, while the zero-point fluctuation $q_0 = \sqrt{\hbar/2m\omega_m}$ characterizes the fundamental quantum limit of the mechanical oscillator with mass $m$ and oscillation frequency $\omega_m$. In this Hamiltonian, the first two terms on the right side represent the free Hamiltonians of the cavity field and mechanical mode. The third term shows the dispersive

optomechanical interaction between cavity field and mechanical mode. With the assumption of strong driving, the last term denotes the interaction between cavity field and classical driving laser.

By moving the Hamiltonian to the rotating framework of laser frequency $\omega_l$, the time-independent Hamiltonian can be written as

$$\begin{aligned}\hat{H}' =&\hbar\Delta_c\hat{a}^\dagger\hat{a}+\frac{1}{2}\hbar\omega_m\left(\hat{p}^2+\hat{q}^2\right)-\hbar G\hat{a}^\dagger\hat{a}\hat{q}\\&+i\hbar E\left(\hat{a}^\dagger-\hat{a}\right),\end{aligned}\tag{2}$$

where $\Delta_c=\omega_c-\omega_l$ is the detuning between the cavity field and the driving laser. Under the interaction picture, the evolution of the operator obeys $\dot{\hat{O}}=\frac{1}{i\hbar}\left[\hat{O},\hat{H}'\right]$, where $\hat{O}=\{\hat{a},\hat{a}^\dagger,\hat{q},\hat{p}\}$. Then the dynamics of the system can be described via the following nonlinear quantum Langevin equations:

$$\dot{\hat{q}}=\omega_m\hat{p},\tag{3}$$

$$\dot{\hat{p}}=-\omega_m\hat{q}-\gamma_m\hat{p}+G\hat{a}^\dagger\hat{a}+\hat{\xi},\tag{4}$$

$$\dot{\hat{a}}=-\kappa\hat{a}-i\Delta_c\hat{a}+iG\hat{a}\hat{q}+E+\sqrt{2\kappa}\hat{a}^{in},\tag{5}$$

where noise operators $\xi$ and $\hat{a}^{in}$ are used to described the fluctuation-dissipation processes. The correlation function of the Hermitian Brownian noise operator $\xi$ is characterized by [46]

$$\left\langle\xi\left(t\right)\xi\left(t'\right)\right\rangle=\frac{\gamma_m}{\omega_m}\int\frac{d\omega}{2\pi}e^{-i\omega\left(t-t'\right)}\omega\left[1+\coth\left(\frac{\hbar\omega}{2k_BT}\right)\right],\tag{6}$$

where $k_B$ is the Boltzmann constant and $T$ is the temperature of the environment. The input vacuum noise $\hat{a}^{in}$ satisfies the delta-correlated relation

$$\left\langle a^{in}\left(t\right)a^{in^\dagger}\left(t'\right)\right\rangle=\delta\left(t-t'\right).\tag{7}$$

Moreover, both noise operators $\xi$ and $\hat{a}^{in}$ are zero-mean.

In this work, the phonon laser generated from the optomechanical interaction by utilizing a mechanical oscillator with a high enough quality factor, satisfying $Q_m=\omega_m/\gamma_m\gg1$. Correspondingly, the Brownian noise $\xi\left(t\right)$ would conform the delta-correlated relation

$$\left\langle\xi\left(t\right)\xi\left(t'\right)\right\rangle=\gamma_m\left(2\bar{n}+1\right)\delta\left(t-t'\right).\tag{8}$$

$\bar{n}=1/(\exp\left(\hbar\omega_m/k_BT\right)-1)$ is the mean phonon number of the mechanical oscillator.

Next, in order to simulate the dynamics of the system, the cavity field operators $\hat{a}^\dagger$ and $\hat{a}$ are resolved into real and imaginary quadratures via $\hat{X}=\left(\hat{a}+\hat{a}^\dagger\right)/\sqrt{2}$ and $\hat{Y}=\left(\hat{a}-\hat{a}^\dagger\right)/i\sqrt{2}$. Similarly, the noise operators are defined as $\hat{X}^{in}=\left(\hat{a}^{in}+\hat{a}^{in\dagger}\right)/\sqrt{2}$ and $\hat{Y}^{in}=\left(\hat{a}^{in}-\hat{a}^{in\dagger}\right)/i\sqrt{2}$, respectively. With such that, Eqs. (3)- (5) can be arranged as

$$\dot{\hat{q}}=\omega_m\hat{p},\tag{9}$$

$$\dot{\hat{p}} = -\omega_m \hat{q} - \gamma_m \hat{p} + G(\hat{X}^2 + \hat{Y}^2)/2 + \hat{\xi}, \tag{10}$$

$$\dot{\hat{X}} = -\kappa \hat{X} + \Delta_c \hat{Y} - G\hat{Y}\hat{q} + \sqrt{2}E + \sqrt{2\kappa}\hat{X}^{in}, \tag{11}$$

$$\dot{\hat{Y}} = -\kappa \hat{Y} - \Delta_c \hat{X} + G\hat{X}\hat{q} + \sqrt{2\kappa}\hat{Y}^{in}. \tag{12}$$

Then, the effective phonon number $N_b$ can be obtained from the view of the mean energy of the mechanical oscillator [47]

$$U = \frac{1}{2}\hbar\omega_m(\langle \delta q^2 + \delta p^2 \rangle) \equiv \hbar\omega_m(N_b + \frac{1}{2}) \tag{13}$$

where $\delta q = q - \langle q \rangle$, $\delta p = p - \langle p \rangle$. The normalized second-order correlation function is introduced to evaluate the coherence of the motional mechanical oscillator. In the condition of the zero time delay, it can be defined as [14,19]

$$g^{(2)}(0) = \frac{\left\langle \hat{b}^\dagger \hat{b}^\dagger \hat{b}\hat{b} \right\rangle}{\left\langle \hat{b}^\dagger \hat{b} \right\rangle^2} = \frac{\langle N_b^2 \rangle - \langle N_b \rangle}{\langle N_b \rangle^2}. \tag{14}$$

The motion of the mechanical oscillator is thermal (coherent) if $g^{(2)}(0) = 2$ ($g^{(2)}(0) = 1$).

In this paper, we adopt a Stochastic Fourth-Order Runge-Kutta method to simulate the evolution of Eqs. (9)-(12). The Stochastic Fourth-Order Runge-Kutta method is a high-order numerical scheme designed to solve the Ito-type stochastic differential equations (SDEs) [46]. Specific simulation methods are present in Appendix A.

## 3. Results

The cavity optomechanical system operates at room temperature and without any external optical or electrical feedback. The dissipative behavior like random collisions with atmospheric molecules gives the positive damping to a free mechanical oscillator. In the absence of driving, the damping would gradually slow down the oscillator's motion until the thermal fluctuations cover its dynamics. In contrast, when the cavity field is excited by the driving laser, the optomechanical interaction can introduce additional damping or gain to the motion of the mechanical oscillator, leading to either cooling or heating effects [40].

As shown in Fig. 1(b), the dimensionless displacement $q$ as a function of the evolution time. At a low driving power $P = 0.1$ mW, the energy transfer from the cavity field is insufficient to overcome the mechanical damping, resulting in a cyclic process of excitation and damping. When the power increases to $P$ =0.4 mW, the dynamics of the mechanical oscillator shows the periodic oscillation in Fig. 1(c). In comparison with Fig. 1(b), the oscillation amplitude has great amplification and its fluctuations remain considerable. As depicted in Fig. 1(d), upon raising the input power to 1.0 mW, the oscillation amplitude grows monotonically until the system enters a self-sustained oscillation regime, in which the thermal fluctuations are strongly suppressed. Overall, there is a threshold power that the motion of the mechanical

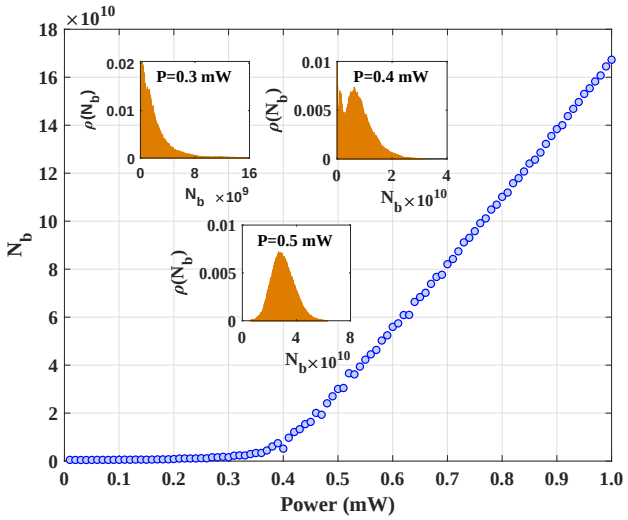



Fig. 2: The effective phonon number $N_b$ as a function of the power $P$. The inset pictures describe the distribution of the effective phonon number with power $P = 0.3$ mW, $P = 0.4$ mW, and $P = 0.5$ mW. Other parameters are the same with Fig. 1.

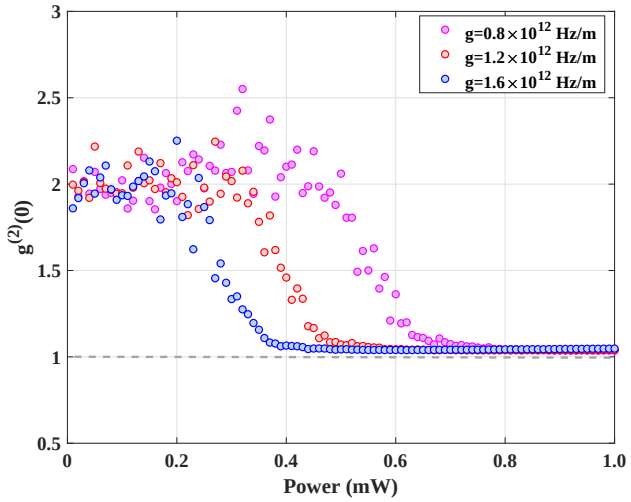



Fig. 3: The normalized second-order correlation function $g^{(2)}(0)$ as a function of the power $P$ with different optomechanical coupling $g$. Parameters are the same with Fig. 1.

oscillator have a dynamical phase transition. In the following, we will systematically investigate the dynamical phase transition through two key optical metrics: the effective phonon number $N_b$ and the normalized second-order correlation function $g^{(2)}(0)$.

It is insufficient to merely consider the dimensionless displacement to understand the dynamical phase transition. The effective phonon number $N_b$ is introduced as a unified metric to characterize the dynamical phase transition through its dual dependence on dimensionless displacement and momentum. As derived from Eq. (13), $N_b$ explicitly incorporates fluctuations in both dimensionless displacement ($\delta q$) and momentum ($\delta p$), providing a comprehensive description to the dynamical phase transition. As shown in Fig. 2, the effective phonon number $N_b$ as a function of the power $P$. With the increase of power $P$, $N_b$ increases monotonically. Notably, a distinct threshold power is observed around $P = 0.4$ mW. Below this threshold value, $N_b$ exhibits gradual growth, whereas above it, a pronounced enhancement in $N_b$ emerges. Furthermore, as evidenced by the inset figures, the effective phonon number distribution $\rho(N_b)$ performs distinct statistical behaviors: the Bose-Einstein distribution at $P = 0.1$ mW and the Poisson distribution at $P = 1.0$ mW, corresponding to the character of thermal motion and coherent behavior, respectively. When power arrives at $P = 0.4$, $\rho(N_b)$ shows a mix of the Bose-Einstein distribution and Poisson distribution. Both thermal and coherent behaviors occur in dynamics.

Another critical way to investigate the dynamical phase transition is the normalized second-order correlation function with zero time delay, $g^{(2)}(0)$, which has been widely applied to research the second-order coherence of the light. Without loss of generality, the normalized second-order correlation function can also be used to character the second-order coherence of the phonons [14,19]. From Fig. 3, $g^{(2)}(0)$ oscillates around 2 at lower power levels. It reflects the competition between the thermal decoherence and the coherent optical force. Under this competition, the stronger optomechanical interactions will result the smaller threshold value of the driving power. With continued growth in optical power, $g^{(2)}(0)$ undergoes a rapid drop, eventually approaching unity. This transition marks the onset of coherent mechanical motion, during which the oscillator's dynamics evolve from thermally driven fluctuations toward phase-stable, laser-like behavior (characterized by Poissonian statistics) [41]. Based on the above discussions, the threshold behavior, together with $g^{(2)}(0) = 1$, confirms the successful preparation of phonon laser in an unresolved sideband [14,19–22].

Within the strong driving, cavity photons are extensively excited through the cavity-driving interaction. The enhanced optical force can shift the mechanical frequency and generate a positive or negative damping on mechanical oscillator [38]. We then examine the phonon laser's behavior in the frequency domain, specifically analyzing its mechanical frequency and damping rate. As illustrated in Fig 4, the power spectral density (PSD) of dimensionless displacement is investigated for varying input powers. When the driving power improves from $P = 0.1$ mW to $P = 1.0$ mW, both the effective mechanical frequency and damping rate are shift from the initial state due to the optical spring effects [40]. More specifically, the mechanical frequency shifts upward from 14.4 kHz to 18.28 kHz and the full width at half maximum of the PSD have a sharp narrowing from 1000 Hz to 9.5 Hz. Moreover, the main peak in PSD shows a

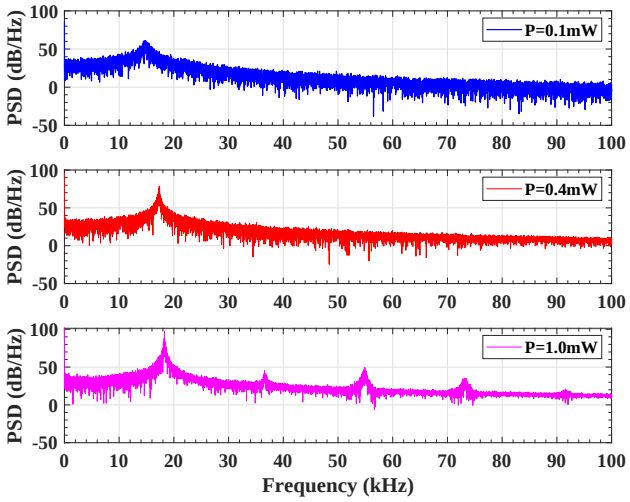



Fig. 4: The power spectral density (PSD) of dimensionless displacement $q$ with power $P = 0.1$ mW , $P = 0.4$ mW, and $P = 1.0$ mW. Other parameters are the same with Fig. 1.

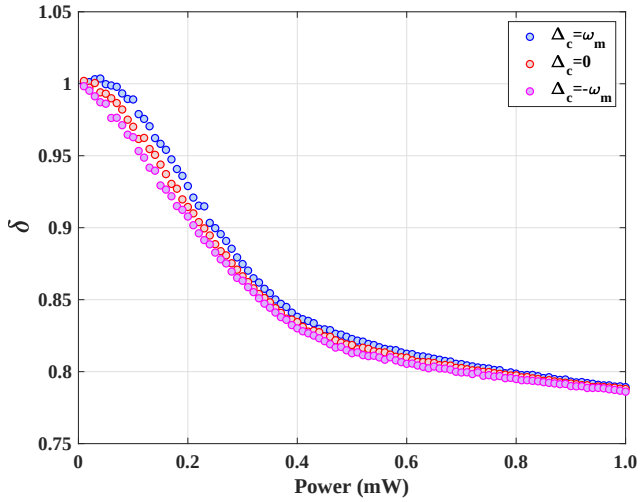



Fig. 5: The ratio $\delta = \sigma(q)/\sigma(p)$ as a function of the power $P$ with different cavity-driving detuning $\Delta_c$. The mechanical oscillator is squeezed if $\delta < 1$. Other parameters are the same with Fig. 1.

remarkable increase of 30 dB, reflecting a substantial mechanical amplification. This significant amplification enhances the nonlinear optomechanical interaction ($\hbar G\hat{a}^{\dagger}\hat{a}\hat{q}$), thereby leading to the higher-order harmonics. By comparing Figs. 2-4, the simultaneous generation of phonon laser with the higher-order harmonics demonstrates that phonon laser originates from the nonlinear optomechanical interaction.

Next, we will explore the nonlinear optomechanical interaction by introducing the ratio $\delta = \sigma(q)/\sigma(p)$, where $\sigma(q)$ and $\sigma(p)$ denote the standard deviation of the dimensionless displacement and momentum. Fig. 5 shows the ratio $\delta$ as a function of the driving power $P$ for different cavity-driving detuning $\Delta_c$. With the growing of the power, $\delta$ decreases monotonically and falls below 1. The reduction indicates the squeezing of the motional oscillator, which occurs regardless of whether the dynamics of the oscillator is in the thermal or coherent behaviors. Combining the discussions of Figs. 2-4, we can conclude that the phonon laser is squeezed via the nonlinear optomechanical interaction. In addition, the phonon laser has a large mean phonon number and operates in a room-temperature thermal environment. The nonlinear optomechanical interaction redistributes the thermal fluctuations between the $\hat{q}$ and $\hat{p}$ quadratures, producing unequal thermal fluctuation in mechanical phase space. Therefore, the observed squeezing of the phonon laser should be understood as thermal squeezing rather than genuine quantum squeezing.

Finally, we explore the thermal squeezed phonon laser from the perspective of the dynamical stability. Generally, in the phase space of a harmonic oscillator, the convergence of trajectories to either a point or a limit cycle confirms the dynamical stability. The transition process from a point attractor to a limit cycle will destabilize the harmonic oscillator [46]. As shown in Fig. 6, the normalized second-order correlation $g^{(2)}(0)$ and the ratio $\delta$ as a function of the cavity quality factor $Q_c$ with different mechanical damping $\gamma_m$. With $Q_c$ going up, the augmentation of photon lifetime will enhance the nonlinear optomechanical interaction, resulting a dynamical phase transition. Around the range of the dynamical phase transition, $\delta$ has a distinct minimum value, which seems counterintuitive to the above discussions that the enhanced optomechanical interaction typically boost the squeezing effect. It can be understood that the maximum squeezing can be attained as the dynamic of the mechanical oscillator approaches the instability, where the two-mode squeezing interaction is significantly enhanced [43–45]. When the squeezed phonon laser is excited, the dynamics of the mechanical oscillator becomes quasi-periodic as shown in Fig. 1(c) and Fig. 4. The metastability of these quasi-periodic oscillations causes $\delta$ to increase gradually beyond the minimum value [46].

From Fig. 6(b), we found that preparing phonon laser in a high mechanical damping rate yields greater squeezing degrees. This phenomenon can also be explained through the dynamical stability analysis. Based on the discussions about Fig 2-4, the optical force provides gain to amplify the mechanical oscillator's motion. The greater damping by the thermal environment, the stronger the optomechanical force required to generate a higher gain for exciting its motion. The motion of the mechanical oscillator will be more unstable during the transition from the thermal motions to the coherent oscillations, thereby sustaining the great squeezing in a high damping rate.

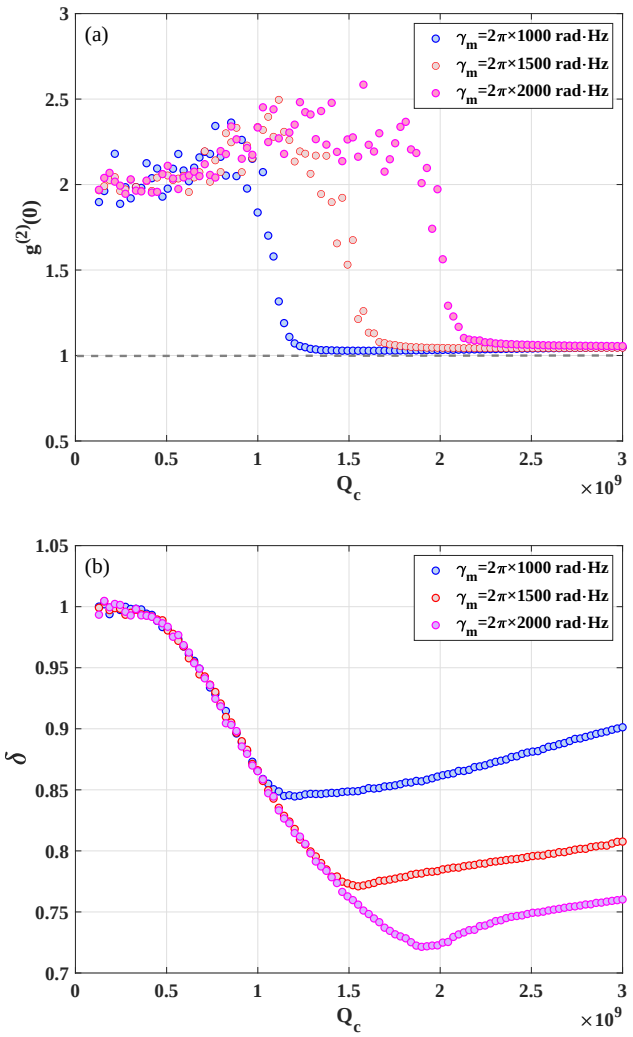



Fig. 6: The normalized second-order correlation function $g^{(2)}(0)$ (a) and the squeezing ratio $\delta$ (b) as a function of the cavity quality $Q_c$ with different mechanical damping $\gamma_m$. The power is given as $P = 0.3$ mW. Other parameters are the same with Fig. 1.

## 4. Conclusion

In summary, we have proposed a theoretical scheme to achieve the thermal squeezed phonon laser via the nonlinear optomechanical interaction at room temperature. In contrast to the two-mode squeezed phonon laser and the bath-free squeezed phonon laser, our proposal operates without any intricate feedback control or detuning modulation [39,48]. This suggests the feasibility of a compact squeezed phonon laser sensor with inherent advantages of structural simplicity. It will give a promising platform for exploring the non-equilibrium physics and nonlinear phononics for precision metrology, including the detection on gravitational wave [49,50], Casimir effect [51–53], and acoustic signal [54,55].

Furthermore, optical cavity with ultrahigh quality factor and unresolved sideband are extremely difficult to satisfy simultaneously. A feasible solution is to design a cavity optomechanical system combining a super-polished end mirror (surface roughness better than 0.1 nm) and a trampoline resonator [56]. Another viable approach is to place phononic density-modulated membranes within a high-finesse Fabry–Pérot cavity [57]. These methods provide easy-to-apply cavity optomechanical systems to realize the squeezed phonon laser, expanding the exploration in sensing [58], heat engines [59], and synchronization in many-body systems [60,61].

## Appendix A: Stochastic Fourth-Order Runge-Kutta Method

We numerically integrate Eqs. (9)-(12) by combining a fourth-order Runge-Kutta treatment of the deterministic drift with properly normalized Wiener increments for the additive Gaussian noises [46]. The vector stochastic differential equation is written in the Ito form

$$d\mathbf{Y}(t) = \mathbf{F}\big(t, \mathbf{Y}(t)\big)dt + \mathbf{B}\, d\mathbf{W}_t, \tag{15}$$

where $\mathbf{F}$ is the drift vector, $\mathbf{B}$ is the noise-amplitude matrix, and $\mathbf{W}_t$ is a vector of independent standard Wiener processes. For Eqs. (9)-(12), the mechanical thermal noise and the two optical vacuum-quadrature noises are additive; therefore, $\mathbf{B}$ is independent of $\mathbf{Y}$.

For a time step $s$, the Wiener increment is

$$\Delta\mathbf{W}_n = \mathbf{W}(t_n + s) - \mathbf{W}(t_n) = \sqrt{s}\,\boldsymbol{\xi}_n, \tag{16}$$

where the components of $\boldsymbol{\xi}_n$ are independent normal random variables with distribution $N(0,1)$. Consequently,

$$\langle \Delta\mathbf{W}_n \rangle = 0, \qquad \big\langle \Delta\mathbf{W}_n \Delta\mathbf{W}_n^T \big\rangle = s\mathbf{I}. \tag{17}$$

An independent vector $\boldsymbol{\xi}_n$ is generated at every time step. This $\sqrt{s}$ scaling is required for a Wiener increment and is used for both the mechanical thermal noise and the optical vacuum noise.

The deterministic Runge-Kutta stages are

$$\mathbf{K}_1 = \mathbf{F}\big(t_n, \mathbf{Y}_n\big), \tag{18}$$

$$\mathbf{K}_2 = \mathbf{F}\left(t_n + \frac{s}{2}, \mathbf{Y}_n + \frac{s}{2}\mathbf{K}_1\right), \tag{19}$$

$$\mathbf{K}_3 = \mathbf{F}\left(t_n + \frac{s}{2}, \mathbf{Y}_n + \frac{s}{2}\mathbf{K}_2\right), \tag{20}$$

$$\mathbf{K}_4 = \mathbf{F}\left(t_n + s, \mathbf{Y}_n + s\mathbf{K}_3\right). \tag{21}$$

The state is then updated according to

$$\mathbf{Y}_{n+1} = \mathbf{Y}_n + \frac{s}{6}\left(\mathbf{K}_1 + 2\mathbf{K}_2 + 2\mathbf{K}_3 + \mathbf{K}_4\right) + \mathbf{B}\Delta\mathbf{W}_n. \tag{22}$$

## Acknowledgment

This research is supported by Quantum Science and Technology-National Science and Technology Major Project (Grant No. 2024ZD0301000), National Natural Science Foundation of China (12474368,12404420), Science Fund for Distinguished Young Scholars of Hunan Province (2024JJ2055), and the Key Science and Technology Breakthrough Program of Hunan Province (2023ZJ1010).

## 参考文献

[1] Li B B, Ou L, Lei Y and Liu Y C 2021 *Nanophotonics* **10** 2799

[2] Xia Y, Agrawal A R, Pluchar C M, Brady A J, Liu Z, Zhuang Q, Wilson D J and Zhang Z 2023 *Nat. Photonics* **17** 470

[3] Wang M, Perez-Morelo D J, Ramer G, Pavlidis G, Schwartz J J, Yu L, Ilic R, Centrone A and Aksyuk V A 2023 *Sci. Adv.* **9** eadf7595

[4] Fogliano F, Besga B, Reigue A, Heringlake P, Mercier de Lépinay L, Vaneph C, Reichel J, Pigeau B and Arcizet O 2021 *Phys. Rev. X* **11** 021009

[5] Huang G, Beccari A, Engelsen N J and Kippenberg T J 2024 *Nature* **626** 512

[6] Kotler S, Peterson G A, Shojaee E, Lecocq F, Cicak K, Kwiatkowski A, Geller S, Glancy S, Knill E, Simmonds R W and others 2021 *Science* **372** 622

[7] Mercier de Lépinay L, Ockeloen-Korppi C F, Woolley M J and Sillanpää M A 2021 *Science* **372** 625

[8] Rossi M, Militaru A, Carlon Zambon N, Riera-Campeny A, Romero-Isart O, Frimmer M and Novotny L 2025 *Phys. Rev. Lett.* **135** 083601

[9] Bonvin E, Devaud L, Rossi M, Militaru A, Dania L, Bykov D S, Romero-Isart O, Northup T E, Novotny L and Frimmer M 2024 *Phys. Rev. Lett.* **132** 253602

[10] Weiss T, Roda-Llordes M, Torrontegui E, Aspelmeyer M and Romero-Isart O 2021 *Phys. Rev. Lett.* **127** 023601

[11] Fiaschi N, Hensen B, Wallucks A, Benevides R, Li J, Alegre T P M and Gröblacher S 2021 *Nat. Photonics* **15** 817

[12] Shandilya P K, Lake D P, Mitchell M J, Sukachev D D and Barclay P E 2021 *Nat. Phys.* **17** 1420

[13] Riedinger R, Wallucks A, Marinković I, Löschnauer C, Aspelmeyer M, Hong S and Gröblacher S 2018 *Nature* **556** 473

[14] Pettit R M, Ge W, Kumar P, Luntz-Martin D R, Schultz J T, Neukirch L P, Bhattacharya M and Vamivakas A N 2019 *Nat. Photonics* **13** 402

[15] Zheng Y, Liu L H, Chen X D, Guo G C and Sun F W 2023 *Phys. Rev. Res.* **5** 033101

[16] Liška V, Zemánková T, Jákl P, Šiler M, Simpson S H, Zemánek P and Brzobohatỳ O 2024 *Nat. Phys.* **20** 1622

[17] Reisenbauer M, Rudolph H, Egyed L, Hornberger K, Zasedatelev A V, Abuzarli M, Stickler B A and Delić U 2024 *Nat. Phys.* **20** 1629

[18] Wang G, Zhao M, Qin Y, Yin Z, Jiang X and Xiao M 2017 *Photonics Res.* **5** 73

[19] Kuang T, Huang R, Xiong W, Zuo Y, Han X, Nori F, Qiu C W, Luo H, Jing H and Xiao G 2023 *Nat. Phys.* **19** 414

[20] Xiao G, Kuang T, He Y, Chen X, Xiong W, Han X, Tan Z, Luo H and Jing H 2024 *eLight* **4** 17

[21] He Y, Kuang T, Han X, Feng Z, Chen X, Xiong W, Jin S, Tan Z, Zhang Q, Luo H and others 2025 *Sci. Adv.* **11** eadv9984

[22] Xiao G, Feng Z, Kuang T, Huang R, He Y, Chen X, Zuo Y, Han X, Xiong W, Tan Z, Ganesan A, Nori F, Qiu C W, Zhang X, Luo H and Jing H 2026 *Advanced Photonics* **8** 026004

[23] Lei C, Wang Z, Yang C, Liu Y and Ren J 2025 *J. Phys. Chem. Lett.* **16** 7630

[24] Marti S, von Lüpke U, Joshi O, Yang Y, Bild M, Omahen A, Chu Y and Fadel M 2024 *Nat. Phys.* **20** 1448

[25] Malia B K, Wu Y, Martínez-Rincón J and Kasevich M A 2022 *Nature* **612** 661

[26] Zhang Q, Wang J, Lu T X, Huang R, Nori F and Jing H 2024 *Sci. China:Phys., Mech. Astron.* **67** 100313

[27] Mashaal A, Stefan L, Ranfagni A, Catalini L, Chernobrovkin I, Capelle T, Langman E C and Schliesser A 2025 *Phys. Rev. Res.* **7** L012071

[28] Gong Z C, Shen C Y, Mao T H, Sun C P, Li Y and Fu H 2023 *Sci. China:Phys., Mech. Astron.* **66** 274211

[29] Lane B B, Chen J, Pagano R E, Aronson S, Cole G D, Yin X, Corbitt T R and Mavalvala N 2024 *arXiv preprint arXiv:2410.09208*

[30] Meng C, Brawley G A, Bennett J S, Vanner M R and Bowen W P 2020 *Phys. Rev. Lett.* **125** 043604

[31] Rashid M, Tufarelli T, Bateman J, Vovrosh J, Hempston D, Kim M S and Ulbricht H 2016 *Phys. Rev. Lett.* **117** 273601

[32] Muffato R, Georgescu T S, Homans J, Guerreiro T, Wu Q, Chisholm D A, Carlesso M, Paternostro M and Ulbricht H 2025 *Phys. Rev. Res.* **7** 013171

[33] Kamba M, Hara N and Aikawa K 2025 *Science* **389** 1225

[34] Youssefi A, Kono S, Chegnizadeh M and Kippenberg T J 2023 *Nat. Phys.* **19** 1697

[35] Lei C U, Weinstein A J, Suh J, Wollman E E, Kronwald A, Marquardt F, Clerk A A and Schwab K C 2016 *Phys. Rev. Lett.* **117** 100801

[36] Wollman E E, Lei C U, Weinstein A J, Suh J, Kronwald A, Marquardt F, Clerk A A and Schwab K C 2015 *Science* **349** 952

[37] Ma X, Viennot J J, Kotler S, Teufel J D and Lehnert K W 2021 *Nat. Phys.* **17** 322

[38] Aspelmeyer M, Kippenberg T J and Marquardt F 2014 *Rev. Mod. Phys.* **86** 1391

[39] Lee C Y and Lin G D 2026 *arXiv:2601.05575*

[40] Leijssen R, La Gala G R, Freisem L, Muhonen J T and Verhagen E 2017 *Nat. Commun.* **8** ncomms16024

[41] Glauber R J 2007 *Quantum theory of optical coherence: selected papers and lectures* (John Wiley & Sons)

[42] Agarwal G S 2012 *Quantum optics* (Cambridge University Press)

[43] Kustura K, Gonzalez-Ballestero C, Sommer A D L R, Meyer N, Quidant R and Romero-Isart O 2022 *Phys. Rev. Lett.* **128** 143601

[44] Genes C, Mari A, Tombesi P and Vitali D 2008 *Phys. Rev. A* **78** 032316

[45] Li G Y, Nie W J, Li X Y, Li M C, Chen A X and Lan Y H 2019 *Sci. China:Phys., Mech. Astron.* **62** 100311

[46] Wang G, Huang L, Lai Y C and Grebogi C 2014 *Phys. Rev. Lett.* **112** 110406

[47] Li G, Nie W, Li X and Chen A 2019 *Phys. Rev. A* **100** 063805

[48] Zhang K, Xiao K, Bhattacharya M and Vamivakas A N 2026 *Nature Communications* **17** 2882

[49] Greve G P, Luo C, Wu B and Thompson J K 2022 *Nature* **610** 472

[50] Hsieh H Y, Chen Y R, Wu H C, Chen H L, Ning J, Huang Y C, Wu C M and Lee R K 2022 *Phys. Rev. Lett.* **128** 073604

[51] Weiss T, Roda-Llordes M, Torrontegui E, Aspelmeyer M and Romero-Isart O 2021 *Phys. Rev. Lett.* **127** 023601

[52] Nie W, Wang L, Wu Y, Chen A and Lan Y 2022 *Sci. China:Phys., Mech. Astron.* **65** 230311

[53] Babar A N, Weis T A S, Tsoukalas K, Kadkhodazadeh S, Arregui G, Vosoughi Lahijani B and Stobbe S 2023 *Nature* **624** 57

[54] Lian J, Xu W, Liang C, Liu F and Wang R 2024 *Meas. Sci. Technol.* **35** 086110

[55] Blésin T, Kao W, Siddharth A, Wang R N, Attanasio A, Tian H, Bhave S A and Kippenberg T J 2024 *Nat. Commun.* **15** 6096

[56] Kleckner D, Pepper B, Jeffrey E, Sonin P, Thon S M and Bouwmeester D 2011 *Opt. Express* **19** 19708

[57] Engelsen N J, Beccari A and Kippenberg T J 2024 *Nat. Nanotechnol.* **19** 725

[58] Javid U A, Rogers S D, Graf A and Lin Q 2021 *Laser Photonics Rev.* **15** 2100166

[59] Klaers J, Faelt S, Imamoglu A and Togan E 2017 *Phys. Rev. X* **7** 031044

[60] Sonar S, Hajdušek M, Mukherjee M, Fazio R, Vedral V, Vinjanampathy S and Kwek L C 2018 *Phys. Rev. Lett.* **120** 163601

[61] Li J, Zhou Z H, Wan S, Zhang Y L, Shen Z, Li M, Zou C L, Guo G C and Dong C H 2022 *Phys. Rev. Lett.* **129** 063605